(Received 24 October 2024, Accepted 26 November 2024, Scheduled 5 December 2024)

Asymmetrical Dual-Dipole Based Optically Transparent Wideband Antenna for Wearable Off-Body Communications

Yanjie Pei, Hongmei Liu*, Jingguo Zhang, and Zhongbao Wang

School of Information Science and Technology, Dalian Maritime University, Dalian 116026, Liaoning, China

ABSTRACT: In the paper, an optically transparent wideband antenna is proposed for wearable off-body communications. It consists of two identical asymmetric dipoles connected by parallel metal plates, and is directly fed through the feeding cable. The dual-dipole system allows for the realization of high front-to-back ratio (FBR) without the need of the ground as a reflecting surface, and size reduction can be obtained. The asymmetric dipole can generate two resonant frequencies, thereby expanding the operated bandwidth. In addition, optical transparency is achieved by slotting the dipole and embedding it in the silicone dielectric. For validation, a prototype is fabricated, which exhibits a size of $0.41\lambda_0 \times 0.14\lambda_0 \times 0.13\lambda_0$. The results show that the prototype has a 10-dB fractional bandwidth (FBW) of 34%, an FBR of more than 14.1 dB, and a cross-polarization ratio of more than 20.8 dB. Within the bandwidth, the gain is larger than 2.79 dBi with the average efficiency of over 60%.

1. INTRODUCTION

With the development of wireless body area networks, wearable antennas have been widely used in the fields of biomedicine, sports, defense, navigation and positioning [1–3]. However, since the design of wearable antennas should consider the factors, such as deformation [4], front-to-back ratio (FBR) [5], and wearing comfort [6, 7], it shows more challenges than the traditional antennas. Especially FBR needs to be as large as possible in case that the excessive electromagnetic leakage does harm to the human body.

Usually, patch antennas [8–11] are good candidates in the application of wearable devices with large FBR since they have directional radiation. However, since the bandwidth of patch antennas is narrow ($< 5\%$), techniques such as multi-mode resonance [9, 10] must be adopted for wideband applications, where slots and shorting pins are necessary. In addition, the wider the bandwidth is, the more complex the structure needs to be implemented. For instance, in [11], the antenna achieves a fractional bandwidth (FBW) of 14% by loading metal rings, stacking patches, slotting, and three port feeding.

Monopole and slot antennas can also be used for designing wearable devices. However, since they exhibit omnidirectional radiation [12, 13], reflected surfaces including ground plane, matesurface (MS), and artificial magnetic conductor (AMC) [14–16] have to be applied to obtain unidirectional radiation with high FBR, such as the work in [14] and [15], where AMC is utilized, and the FBR is increased from 0 to 12 dB and 18.5 dB, respectively.

No matter patch or monopole antennas, due to the existence of reflected surfaces which are generally larger than the radiators themselves, the overall size of the antenna is big. For example, in [9], the ground is 2.8 times larger than the radiator. In [14], the size of the radiator is $0.29 \times 0.29\lambda^2$, while the size of the AMC plane is $1.44 \times 0.46\lambda^2$. Thus, it is found that the size of the reflector is the main factor that influences the overall size of the wearable antenna.

Recently, based on backward field cancellation theory, a dual-dipole system is presented to realize unidirectional radiation [17]. Since antennas do not contain large reflected surfaces, the size of the antenna is determined by the radiator. Results show that dimension of the antenna is only $0.46\lambda \times 0.06\lambda$, and the FBR is greater than 9.8 dB at the center frequency. The drawbacks are that the narrow bandwidth (1.6%) limits its wideband application, and the radiation efficiency is lower (maximum 50%).

In this article, an asymmetrical dual-dipole system is proposed for realizing wearable antenna with wide bandwidth, high FBR, and small size. In addition, unlike the general wearable antenna which employs textile material as medium [18–20], the proposed antenna employs a silica gel medium which has higher dielectric constant (the textile material is 1.38, and the silicone media is 2.75) and optically transparent feature. Compared to textile antennas, transparent wearable antennas [21–23], with the potential ability to increase their esthetic appeal and the comfort of the wearer through visually unnoticeable and flexible, are better options in terms of application scenarios, such as smart glasses and flexible solar cells. However, the reported transparent wearable antennas have their own shortcomings. For example, the transparent antenna in [21] has a narrow bandwidth of only 0.07%. The transparent wearable antenna proposed in [22] achieves a wide bandwidth, but the efficiency is low ($< 50\%$). To solve the problem of narrow bandwidth and low efficiency of transparent wearable antennas, the asymmetrical dual dipoles are embedded in the silica gel medium in the design. Measurements show that the antenna

* Corresponding author: Hongmei Liu (lhm323@dlmu.edu.cn).

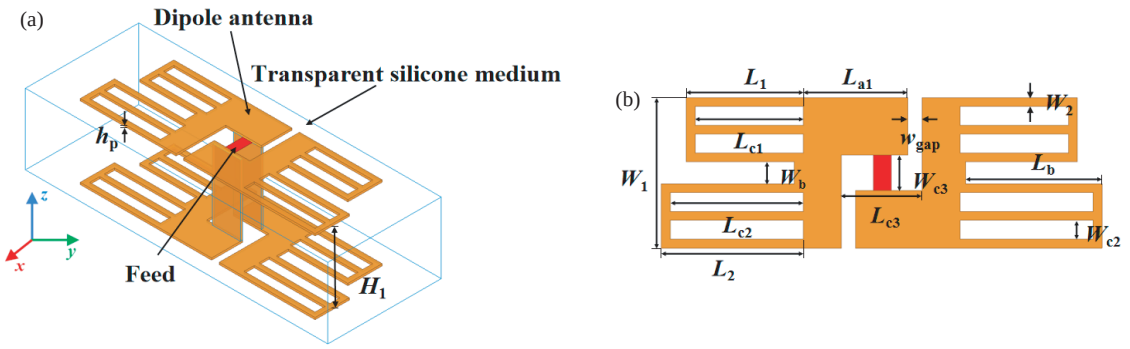

FIGURE 1. Configuration of the proposed antenna. (a) 3-D view. (b) Top view of radiant part.

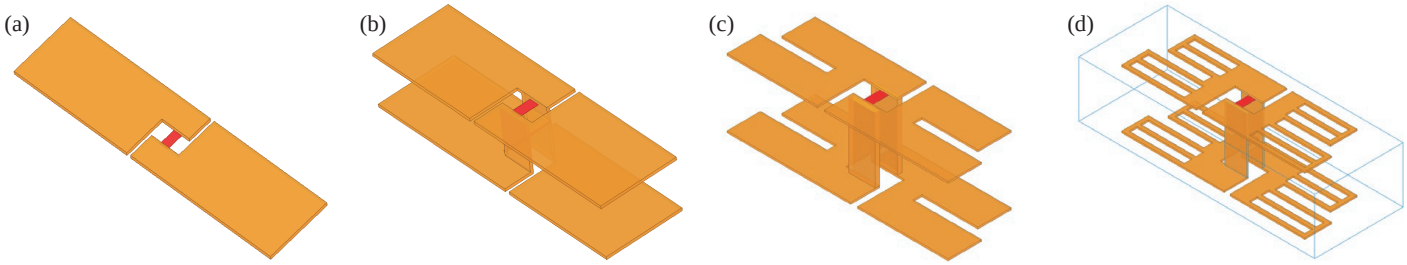

FIGURE 2. Evolutions of the proposed antenna. (a) Ant. 1. (b) Ant. 2. (c) Ant. 3. (d) Ant.4.

achieves a 10-dB FBW of 32.4% with FBR greater than 14 dB and cross-polarization more than 17 dB. The maximum radiation efficiency of the proposed antenna reaches 70.2%.

2. ANTENNA CONFIGURATION AND DESIGN PROCEDURE

2.1. Configuration of the Proposed Antenna

Figure 1 illustrates the configuration of the proposed wearable antenna, where the radiator consists of two same dipoles connected by parallel metal plate and embedded in a transparent silicone medium ($\varepsilon_r = 2.75$, $\tan\delta = 0.05 \sim 0.07$, $h = H_1 + 2h_p$). The dipole antenna and parallel metal plate are both copper plates with $h_p = 0.2$ mm thickness. The parallel metal plates with size $H_1 \times (L_{c3} - w_{\text{gap}})$ are used to connect the upper and lower dipole antennas. To expend the bandwidth, each of the dipoles is composed of two unequal arms connected by an L-shaped metal plate. The sizes of the long and short arms are $L_2 \times (W_1 - W_b)/2$ and $L_1 \times (W_1 - W_b)/2$, respectively. On the basis, two rectangular slots with the dimensions of $L_{c2} \times W_{c2}$ and $L_{c1} \times W_{c2}$ are cut on the long and short arms, respectively for improving the optical transparency of the antenna. The L-shaped metal plate consists of vertically connected rectangle 1 and rectangle 2 with dimensions of $(L_{a1} + w_{\text{gap}} - L_{c3}) \times W_1$ and $(L_{c3} - w_{\text{gap}}) \times (W_1 - W_{c3})/2$. It is noted that the excitation is performed between the two L-shaped metal plates. After optimization using the HFSS, final dimensions of the proposed antenna are shown in Table 1.

TABLE 1. Dimensions of the proposed antenna.

Parameters	L_1	W_1	L_2	L_{a1}	L_{c1}	L_{c2}	L_{c3}	W_{c2}
Size (mm)	6.6	8.5	8	5.9	6.1	7.5	4.55	1.065
Parameters	W_{c3}	W_2	L_b	W_b	w_{gap}	h_p	H_1	-
Size (mm)	2	0.5	7.5	1.24	0.75	0.2	7.5	-

2.2. Evolution of the Antenna

Figure 2 presents the evolution of the proposed antenna to illustrate the method of bandwidth and FBR enhancement. The corresponding performances are shown in Fig. 3, including $|S_{11}|$ and radiation patterns at 5.8 GHz.

At the beginning, a simple dipole antenna (named as Ant. 1) is designed at the center frequency of 5.8 GHz, as shown in Fig. 2(a). The dipole length can be roughly calculated as $\lambda_0/2$, where λ_0 is the wavelength in the air. As seen in Fig. 3, the 10-dB FBW is 9.8%, and the FBR is 0.

To increase the FBR, another dipole is set beneath Ant. 1, where the two dipoles are connected through a parallel metal plate (named as Ant. 2). Fig. 2(b) shows the structure of Ant. 2. It is noted that when the distance between the two dipoles is H_1, the parallel metal plate can provide a phase difference of $(\pi + \beta \times H_1)$ (where β is the propagation constant in free space). For the forward radiation, if the radiation phase of the top dipole is 0, the corresponding radiation phase for the bottom dipole is $(\pi + 2 \times \beta \times H_1)$. Then, front unidirectional radiation can be obtained when H_1 is unequal with half-wavelength, and the closer the H_1 is to a quarter-wavelength, the stronger the forward radiation is.

For the backward radiation, the phases of the top and bottom antennas are $(-\beta \times H_1)$ and $(-\pi - \beta \times H_1)$, respectively. As can be seen, the sum of the two phases is always equal to π no matter what is the value of H_1. Thus, the backward radiation is always null in theory, while in realization, due to the multi-

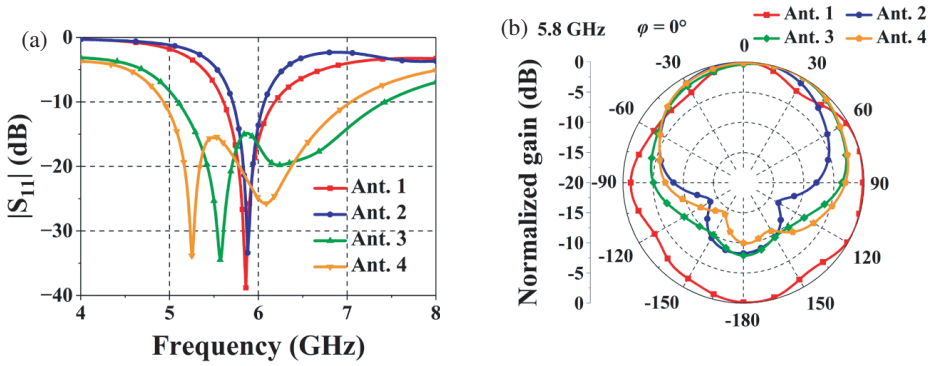

FIGURE 3. Simulated results of the four evolutions. (a) $|S_{11}|$. (b) FBR.

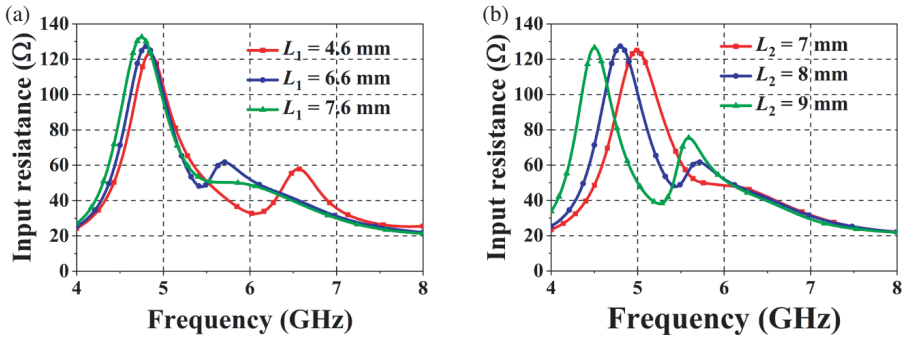

FIGURE 4. Effects of (a) L_1 and (b) L_2 on input resistance.

ple reflections, the backward radiation can be reduced but not eliminated.

As can be seen in Fig. 3, the FBR of Ant. 2 is increased to 8.2 dB, and the 10-dB FBW is 6.1%, which indicates that the adoption of dual dipoles can enhance the FBR significantly without affecting the impedance matching.

For bandwidth enhancement, each arm of the dipole is divided into two arms with different lengths (Ant. 3), as shown in Fig. 2(c). Since dipoles with different arm lengths can resonate at different frequencies, when the two resonant frequencies are close enough by tuning the arm length, the bandwidth of the dipole can be improved effectively. As can be seen in Fig. 3(a), the 10-dB FBW of Ant. 3 is increased to 34.1%, while the FBR is nearly un-influenced.

On the basis, the arm of Ant. 3 is slotted, and the antenna is wrapped with transparent silicone (named Ant. 4) for increasing the optical transparency of the antenna and improving the wearing comfort. The slotting is done along the current direction for not affecting the performance of the antenna. Finally, transparent silicone is poured, and the antenna is wrapped in it. Since the medium between the upper and lower antennas is changed from air ($\varepsilon_r = 1$) to silica gel ($\varepsilon_r = 2.75$), the antenna height is further lowered for size reduction. Besides, the FBR is slightly increased to 9.6 dB.

3. PARAMETER ANALYSIS

To provide further clarification regarding the design mechanism of the proposed antenna, this section will analyze the main parameters in detail. It is noted that the remaining parameters are fixed at their final optimized values throughout the course of the analysis.

3.1. Effect of Arm Length L_1 and L_2

Figure 4 illustrates the effects of arm length (L_1 and L_2) on the resonate frequency. It can be seen from Fig. 4(a) that as L_1 changes from 4.6 mm to 7.6 mm, the impedance peak of the higher resonance shifts from 5 GHz to 6.5 GHz. Correspondingly, the impedance peak of the lower resonance moves from 4.5 GHz to 5 GHz when L_2 varies from 7 mm to 9 mm, as shown in Fig. 4(b). When the two resonant frequencies are close enough, the bandwidth can be broadened. Fig. 5 gives the simulated results of several groups of L_1 and L_2. When $L_1 = 6.6$ mm and $L_2 = 8$ mm, a 10-dB bandwidth from 5.1 GHz to 7.2 GHz can be realized.

3.2. Effect of H_1

From the evolution, it is found that the height of the parallel metal plate affects the antenna FBR. In the air medium, it is calculated that the closer the H_1 is to quarter-wavelength, the better the antenna FBR performance is. For wideband operation, the value of H_1 should be adjusted for obtaining high FBR within the bandwidth. Fig. 6 investigates the normalized radiation patterns of the antenna at four in-band frequencies. It is seen that the FBR varies with both frequency and H_1. At 5.5 GHz, 6 GHz, and 6.5 GHz, the FBR increases with the increase of H_1, while at 7 GHz, the FBR decreases slightly with

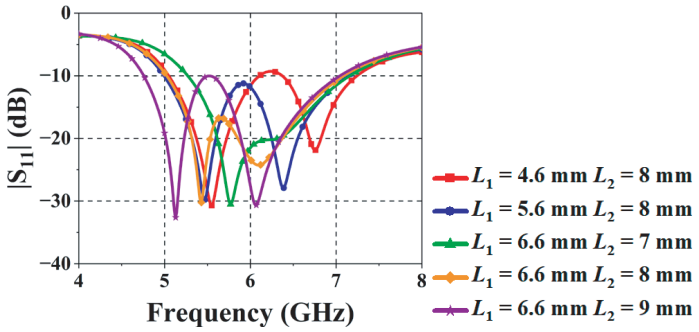

FIGURE 5. Effect of L_1 and L_2 on $|S_{11}|$.

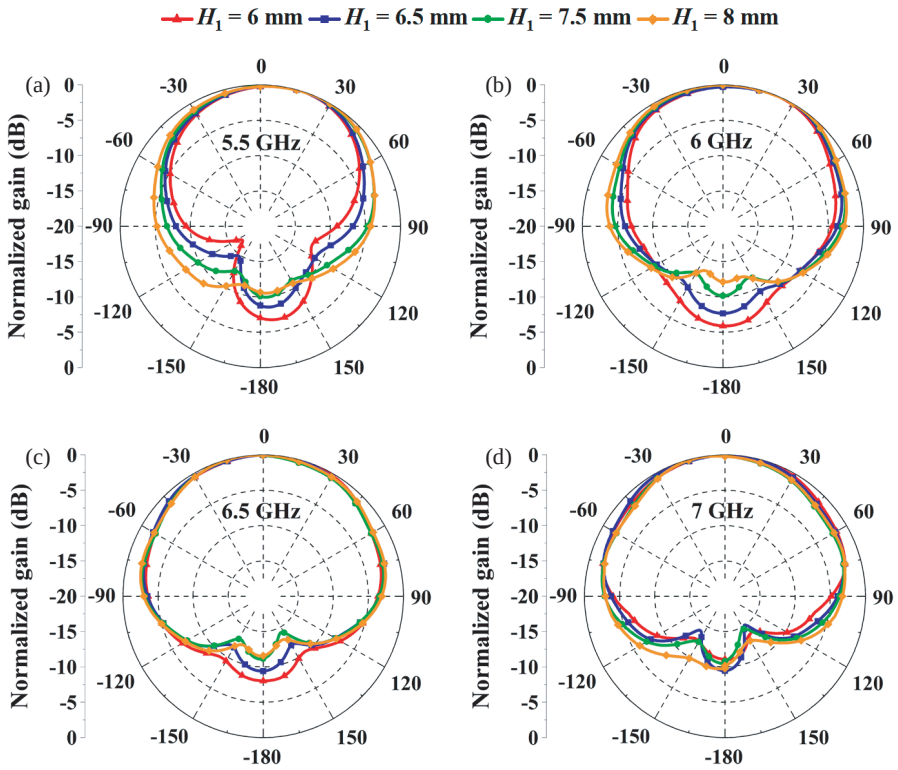

FIGURE 6. Effect of H_1 on FBR. (a) 5.5 GHz. (b) 6 GHz. (c) 6.5 GHz. (d) 7 GHz.

the increase of H_1. Considering the FBR and size, the final value of H_1 is determined as 7.5 mm.

4. EXPERIMENTAL RESULTS

To verify the correctness of the simulation, a prototype was fabricated and rigorously tested. Fig. 7 shows photographs of the prototype. The fabricating procedure is as follows: (1) processing the metal-plate-based dipole and fixing the two dipoles by soldering the feed cable between the L-shaped metal plates. (2) placing the antenna into a mould and pouring the uncured silicone liquid and hardenner, with a ratio of 10:1, into the mould. (3) waiting 24 hours at room temperature, the silicone can be solidified, and the fabrication processing is finished. Figure 8 shows the actual test environment, using a piece of fresh pork to simulate the human body and covering it with a layer of felt. The antenna was placed on top of the felt and fixed with paper tape for testing purposes.

Figure 9 demonstrates the simulated and measured results of the prototype. Under the criterion of $|S_{11}| < -10$ dB, the bandwidth of the antenna is in the range of 5.1 to 7.2 GHz (34%). In this bandwidth, the gain is larger than 2.79 dBi with the peak gain of 3.82 dBi, as seen in Fig. 9(b). Besides, the antenna shows good radiation efficiency, reaching a maximum radiation efficiency of 70.2% and an average efficiency of 60%. The differences between the simulated and measured data can be attributed to the inherent errors generated by the soldering assembly during the antenna fabrication process.

Figure 10 illustrates the radiation patterns of the antenna at two main planes ($\varphi = 0°$ and $\varphi = 90°$). Here, four frequencies (5.5 GHz, 6 GHz, 6.5 GHz, and 7 GHz) are plotted. It is seen that the radiation patterns are stable in the operated bandwidth.

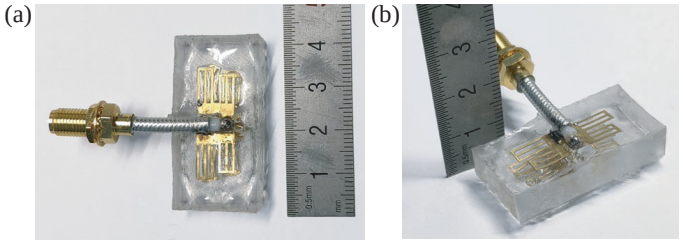

FIGURE 7. Photograph of the fabricated prototype. (a) Top view. (b) 3D view.

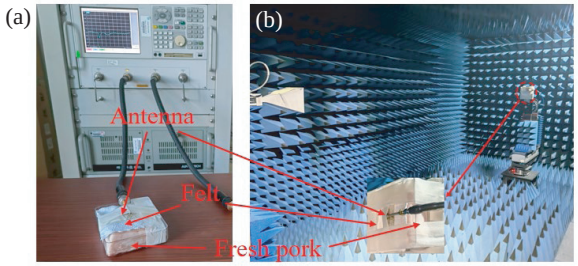

FIGURE 8. Photographs of environment setups. (a) Agilent N5230A vector network analyzer. (b) Anechoic chamber.

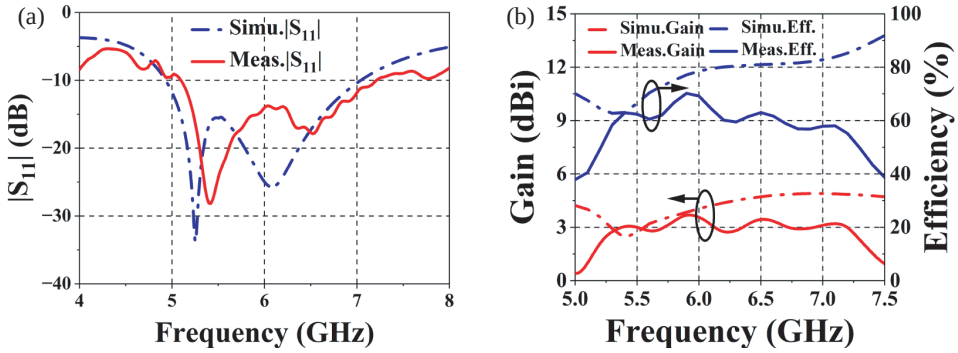

FIGURE 9. Simulated and measured results. (a) $|S_{11}|$. (b) Gain and efficiency.

TABLE 2. Comparison of the designed antenna with other antennas.

Ref.	Overlapped FBW (%)	Peak gain (dBi)	Peak efficiency (%)	FBR (dB)	Dimensions ($\lambda_0 \times \lambda_0 \times \lambda_0$)	Optically transparent (Y/N)
[9]	18	5.9	74.1	10*	$0.79 \times 0.61 \times 0.03$	N
[11]	14	10.8	93	11*	$0.54 \times 0.61 \times 0.09$	N
[14]	24.4	10.59	85	25	$1.44 \times 0.46 \times 0.05$	N
[15]	27.6	5.9	66.1	18.5	$0.64 \times 0.64 \times 0.03$	N
[17]	1.6	4.3	50.1	9.8	$0.46 \times 0.06 \times 0.04$	N
[21]	0.07	3.2	51	10	$0.49 \times 0.49 \times 0.11$	Y
[22]	10.4/20.4	3.2/3.5	46/48	15*	$0.67 \times 0.77 \times 0.06$	Y
This work	34	3.82	70.2	14.1	$0.41 \times 0.14 \times 0.13$	Y

* Estimated from the results. λ_0 is the wave length at the lowest operating frequency.

The measured FBRs of the antenna are 16 dB@5.5 GHz, 17.4 dB@6 GHz, 20.1 dB@6.5 GHz and 14.1 dB@7 GHz. Besides, the measured cross-polarization ratios are 22.1 dB, 20.8 dB, 17.4 dB, and 21.5 dB for the four frequencies, which indicates good linear polarization characteristic.

The specific absorption rate (SAR) simulation is established, and the model is shown in Fig. 11(a). The clothed human body was simulated by modelling four layers: felt, skin, fat, and muscle. Fig. 11(b) plots the SAR values at 5.5 GHz, 6 GHz, 6.5 GHz, and 7 GHz. It is seen that the SAR values are less than 0.8 W/kg per 1 g tissue and less than 0.2 W/kg per 10 g tissue. Both the results are lower than the US (1.6 W/kg per 1 g tissue) and EUR (2 W/kg per 10 g tissue) standards, which indicates that the designed antenna is safe for wearing on human body.

Table 2 compares the performances of the proposed and representative wideband wearable antennas. The proposed antenna shows wider bandwidth and smaller size than the works in [9, 11, 14, 15] using reflected surfaces for unidirectional radiation. Besides, the FBR of the proposed structure is higher than [9] and [11]. Compared with [17] where dual-dipole theory is adopted, the proposed antenna exhibits a big increase of the bandwidth. In addition, the efficiency and FBR within the band are also higher than the antenna in [17]. Compared with the transparent wearable antennas in [21] and [22], the proposed antenna shows wider bandwidth, higher gain and efficiency. Besides, the size of the proposed structure is smaller than those

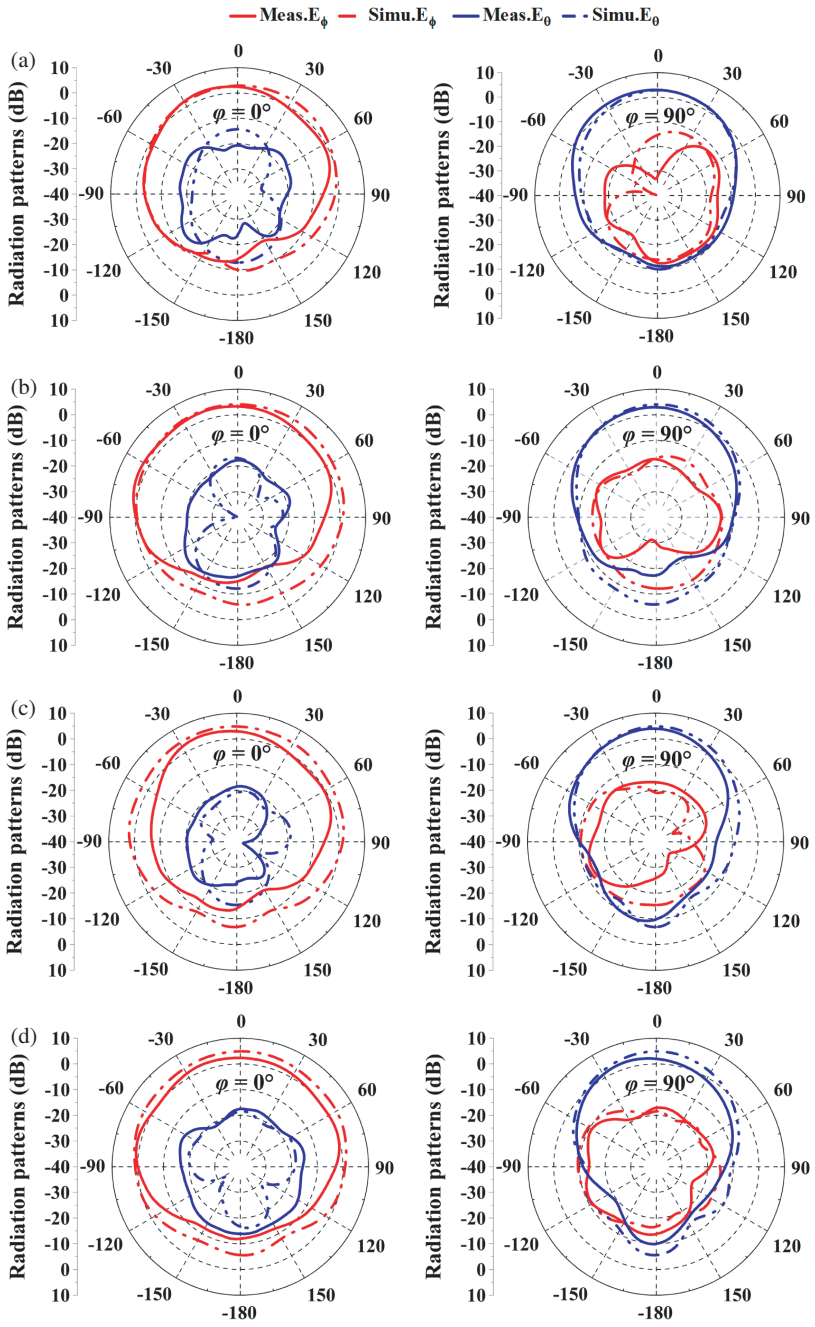

FIGURE 10. Simulated and measured radiation patterns at $\varphi = 0°$ and $\varphi = 90°$. (a) 5.5 GHz. (b) 6 GHz. (c) 6.5 GHz. (d) 7 GHz.

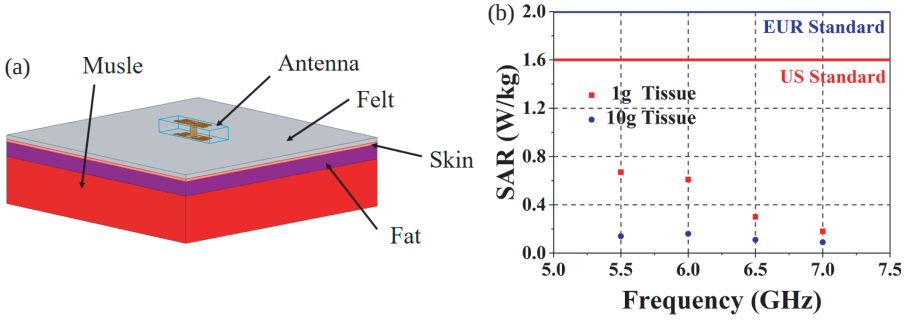

FIGURE 11. SAR simulation. (a) Human tissue cubic model. (b) SAR results at 5.5 GHz, 6 GHz, 6.5 GHz and 7 GHz.

in [21] and [22]. Thus, due to the superior performance of the proposed antenna, it has a broad application scenario in the field of wideband wearable devices.

5. CONCLUSION

In the paper, a wearable antenna with wideband, high FBR, and optical transparency is proposed, which is attributed to the asymmetric dual-dipole system and silica gel medium. Measurement results show that the antenna achieves a 10-dB FBW of 34% with more than 14 dB FBR and 17 dB cross-polarization. Besides, it also shows the advantages of small size, good radiation efficiency, and optically transparent feature, which has broad application prospect in wideband wearable field.

ACKNOWLEDGEMENT

This work was supported in part by the National Natural Science Foundation of China under Grant 52471371, in part by the Young Elite Scientists Sponsorship Program by CAST under Grant 2022QNRC001, in part by the China Scholarship Council, and in part by the Fundamental Research Funds for the Central Universities under Grant 3132024239.

REFERENCES

[1] Yang, S., L. Zhang, W. Wang, and Y. Zheng, "Flexible tri-band dual-polarized MIMO belt strap antenna toward wearable applications in intelligent internet of medical things," *IEEE Transactions on Antennas and Propagation*, Vol. 70, No. 1, 197–208, 2022.

[2] Zaidi, N. I., N. H. A. Rahman, M. F. Yahya, M. S. A. Nordin, S. Subahir, Y. Yamada, and A. Majumdar, "Analysis on bending performance of the electro-textile antennas with bandwidth enhancement for wearable tracking application," *IEEE Access*, Vol. 10, 31 800–31 820, 2022.

[3] Zheng, W., H. Li, and G. Liu, "Design of circularly polarized smartwatch antenna with reactive loads," *IEEE Antennas and Wireless Propagation Letters*, Vol. 22, No. 7, 1602–1606, 2023.

[4] Simorangkir, R. B. V. B., A. Kiourti, and K. P. Esselle, "UWB wearable antenna with a full ground plane based on PDMS-embedded conductive fabric," *IEEE Antennas and Wireless Propagation Letters*, Vol. 17, No. 3, 493–496, 2018.

[5] Yu, S.-W., X. Zhang, Q.-S. Wu, L. Zhu, T. Yuan, and Q.-H. Jiang, "Low-SAR and high-FBR patch antenna with small ground size for wearable devices," *IEEE Open Journal of Antennas and Propagation*, Vol. 5, No. 1, 124–129, 2024.

[6] Dang, Q. H., S. J. Chen, D. C. Ranasinghe, and C. Fumeaux, "Dual-band reconfigurable flexible antenna with independent frequency tunability," *IEEE Antennas and Wireless Propagation Letters*, Vol. 22, No. 3, 531–535, 2023.

[7] Ashyap, A. Y. I., S. H. B. Dahlan, Z. Z. Abidin, M. H. Dahri, H. A. Majid, M. R. Kamarudin, S. K. Yee, M. H. Jamaluddin, A. Alomainy, and Q. H. Abbasi, "Robust and efficient integrated antenna with EBG-DGS enabled wide bandwidth for wearable medical device applications," *IEEE Access*, Vol. 8, 56 346–56 358, 2020.

[8] Sun, H., Y. Hu, R. Ren, L. Zhao, and F. Li, "Design of pattern-reconfigurable wearable antennas for body-centric communications," *IEEE Antennas and Wireless Propagation Letters*, Vol. 19, No. 8, 1385–1389, 2020.

[9] Gao, G.-P., C. Yang, B. Hu, R.-F. Zhang, and S.-F. Wang, "A wide-bandwidth wearable all-textile PIFA with dual resonance modes for 5 GHz WLAN applications," *IEEE Transactions on Antennas and Propagation*, Vol. 67, No. 6, 4206–4211, 2019.

[10] Radavaram, S., S. Naik, and M. Pour, "Stably polarized wideband circular microstrip antenna excited in TM12 mode," *IEEE Transactions on Antennas and Propagation*, Vol. 69, No. 4, 2370–2375, 2021.

[11] Zhang, K., Z. H. Jiang, W. Hong, and D. H. Werner, "A low-profile and wideband triple-mode antenna for wireless body area network concurrent on-/off-body communications," *IEEE Transactions on Antennas and Propagation*, Vol. 68, No. 3, 1982–1994, 2020.

[12] Yu, Z., R. Niu, G. Zhang, R. Sun, Z. Lin, Y. Li, and X. Ran, "A wearable self-grounding slit antenna for ISM/4G/5G/bluetooth/WLAN applications," *IEEE Access*, Vol. 11, 87 930–87 937, 2023.

[13] Le, T. T. and T.-Y. Yun, "Miniaturization of a dual-band wearable antenna for WBAN applications," *IEEE Antennas and Wireless Propagation Letters*, Vol. 19, No. 8, 1452–1456, 2020.

[14] Dey, A. B., S. Kumar, W. Arif, and J. Anguera, "Elastomeric textile substrates to design a compact, low-profile AMC-based antenna for medical and IoT applications," *IEEE Internet of Things Journal*, Vol. 10, No. 6, 4952–4969, 2023.

[15] He, P.-Y., F.-P. Lai, and Y.-S. Chen, "Sensitivity enhancement in cardio-pulmonary stethoscope applications through artificial magnetic conductor-backed antenna design," *IEEE Journal of Electromagnetics, RF and Microwaves in Medicine and Biology*, Vol. 8, No. 2, 135–143, 2024.

[16] El Atrash, M., M. A. Abdalla, and H. M. Elhennawy, "A wearable dual-band low profile high gain low SAR antenna AMC-backed for WBAN applications," *IEEE Transactions on Antennas and Propagation*, Vol. 67, No. 10, 6378–6388, 2019.

[17] Gao, S., L. Chang, and A. Zhang, "Novel unidirectional radiation principle by backward field cancelation and its application to wearable IoT devices," *IEEE Antennas and Wireless Propagation Letters*, Vol. 22, No. 12, 3037–3041, 2023.

[18] Casula, G. A., G. Montisci, and G. Muntoni, "A novel design for dual-band wearable textile eighth-mode SIW antennas," *IEEE Access*, Vol. 11, 11 555–11 569, 2023.

[19] Dang, Q. H., S. J. Chen, D. C. Ranasinghe, and C. Fumeaux, "A frequency-reconfigurable wearable textile antenna with one-octave tuning range," *IEEE Transactions on Antennas and Propagation*, Vol. 69, No. 12, 8080–8089, 2021.

[20] Çelenk, E. and N. T. Tokan, "All-textile on-body antenna for military applications," *IEEE Antennas and Wireless Propagation Letters*, Vol. 21, No. 5, 1065–1069, 2022.

[21] Sayem, A., R. B. V. B. Simorangkir, K. P. Esselle, R. M. Hashmi, and H. Liu, "A method to develop flexible robust optically transparent unidirectional antennas utilizing pure water, PDMS, and transparent conductive mesh," *IEEE Transactions on Antennas and Propagation*, Vol. 68, No. 10, 6943–6952, 2020.

[22] Sayem, A., R. B. V. B. Simorangkir, K. P. Esselle, and R. M. Hashmi, "Development of robust transparent conformal antennas based on conductive mesh-polymer composite for unobtrusive wearable applications," *IEEE Transactions on Antennas and Propagation*, Vol. 67, No. 12, 7216–7224, 2019.

[23] Zhu, W., X. Liu, Y. Fan, Z. Zhang, and X. Ma, "Transparent and flexible antenna with polarization reconfigurability using EGaIn for wearable applications," *IEEE Transactions on Antennas and Propagation*, Vol. 72, No. 10, 7493–7503, 2024.